Acta Metallurgica Sinica (English Letters) (2020) 33:1077–1090
https://doi.org/10.1007/s40195-020-01002-6

Effects of Ti and Cu on the Microstructure Evolution of AlCoCrFeNi High-Entropy Alloy During Heat Treatment

Yuan Yu[1,2] · Peiying Shi[1] · Kai Feng[3] · Jiongjie Liu[1] · Jun Cheng[1] · Zhuhui Qiao[1,2] · Jun Yang[1] · Jinshan Li[4] · Weimin Liu[1]

Received: 15 October 2019 / Revised: 26 November 2019 / Published online: 14 January 2020

Abstract

The microstructure evolution of AlCoCrFeNiTi$_{0.5}$ alloy and AlCoCrFeNiCu alloy during heat treatment was systematically studied, to reveal the influence rules of chemical activity of adding element on the microstructure evolution of AlCoCrFeNi system. Owing to the negative mixing enthalpy with the constituent elements, Ti element was mainly dissolved in the Al–Ni-rich phases, and aggravated the lattice distortion of B2 phase. The structure variation of BCC phase by adding Ti inhibited the formation of FCC phase and enhanced the precipitation of σ phase during heat treatment. Owing to the positive mixing enthalpy with constituent elements, Cu element tended to be repelled to the ID region and formed metastable Cu-rich FCC1 phase which would transform into Cu–Al–Ni-rich FCC2 phase with increasing temperature. The addition of Cu inhibited the precipitation of σ phase during heat treatment. Adding Ti maintained the stable dendritic morphology, while adding Cu reduced the thermal stability of microstructure. Two dramatic morphology changes occurred at 1000 °C and 1100 °C in the AlCoCrFeNiCu alloy. The lattice distortion of phase in AlCoCrFeNiTi$_{0.5}$ alloy was aggravated with increasing temperature up to 800 °C, then relaxed together with the dissolution of σ phase when temperature was above 900 °C. The variation in lattice distortion dominated the hardness of AlCoCrFeNiTi$_{0.5}$ alloy. With increasing heating temperature, the increasing volume fraction of region with FCC structure due to the transformation between FCC phases, and the pronounced coarsening in microstructure due to the reduced thermal stability, resulted in the mainly decreasing trend in the hardness of AlCoCrFeNiCu alloy.

Keywords High-entropy alloy · Heat treatment · Microstructure evolution · Enthalpy · Hardness

1 Introduction

Today, the rapid development of high-tech industries requires structural and tool materials maintaining stabilized operational properties under high temperature, dynamic load and serious wear work conditions. In order to enhance the operational properties, traditional industrial metal with one main solvent element needs to add several alloying additives, which usually degenerate the thermodynamic stability. Under complex and fluctuant environment, phase transformation in conventional metals tends to occur and deteriorate the operational properties [1]. As a revolution in metallurgy fields, high-entropy alloy (HEA) is one of the most promising classes of metals related to the increasing demands of modern industry [2, 3]. HEAs contain at least four equiatomic or near-equiatomic elements, to achieve the high configurational entropy which could stabilize solid solutions with close-packed structures, such as face-centered cubic (FCC), body-centered cubic (BCC) or hexagonal

Available online at http://link.springer.com/journal/40195.

✉ Zhuhui Qiao
zhqiao@licp.cas.cn

✉ Jinshan Li
ljsh@nwpu.edu.cn

1 State Key Laboratory of Solid Lubrication, Lanzhou Institute of Chemical Physics, Chinese Academy of Sciences, Lanzhou 730000, China

2 Qingdao Center of Resource Chemistry and New Materials, Qingdao 266000, China

3 State Key Laboratory of Advanced Design and Manufacturing for Vehicle Body, Hunan University, Changsha 410082, China

4 State Key Laboratory of Solidification Processing, Northwestern Polytechnical University, Xi'an 710072, China

close-packed (HCP), by reducing the Gibbs free energy [4-6]. Summarized by many researchers [7-12], high entropy effect, the cocktail effect, severe lattice distortion and the sluggish diffusion are found in HEAs. With the unique structural features, HEAs reportedly exhibit good mechanical properties, high thermal stability, outstanding resistance to wear, corrosion and fatigue [13-16].

The most extensively investigated HEAs focused on FCC CoCrFeNi system, BCC AlCoCrFeNi system as well as eutectic $AlCoCrFeNi_{2.1}$ system [12-17]. The CoCrFeNi system with solid solution structure exhibited good ductility, and was able to experience deformation-induced nano-twinning to achieve excellent strength–ductility combinations as well as outstanding fracture-toughness at cryogenic temperatures [18, 19]. The eutectic $AlCoCrFeNi_{2.1}$ system showed good liquidity and castability to avoid internal defects and compositional segregations in the large-scale industrial production [20], reached the balanced strength and ductility in a wide temperature range [21, 22], and realized the bulk ultrafine-microstructure materials via direct solidification [23]. The AlCoCrFeNi system with modulated spinodal-like structure obtained good mechanical properties, such as AlCoCrFeNi alloy with ultimate compressive strength of about 2800 MPa and elongation above 20% [24, 25]. Recently, most literature focused on the CoCrFeNi system and eutectic $AlCoCrFeNi_{2.1}$ system. The main reasons responsible for the underestimation of the AlCoCrFeNi system were that micro-cracking occurs at the corner of nano-sized AlNi-rich B2 phase [26], especially during machining and thermo-mechanical processes.

Composition adjustment and post-processing could effectively optimize the microstructure of metals [27-30]. One of the ideal ways to solve this issue of AlCoCrFeNi system should be composition adjustment followed by heat treatment. Comprehensive investigations about HEAs have revealed that the high configuration entropy could stabilize the simple structure, whereas the microscopic structure could be controlled by the mixing enthalpy which dominates the driving force of nucleation in local regions [31, 32]. The additives owning different mixing enthalpies with the constituent elements could not only change the microstructural morphology, but also affect the structure characters of primordial phases [7]. In addition, the mixing enthalpy between different elements and the affected structure characters would further play important roles in the following microstructure evolution during post-processing [33]. Thus, recognizing the relationship between the chemical activity of additives and microstructure evolution during heat treatment is indispensable for effectively optimizing the structure to eliminate micro-cracking of AlCoCrFeNi system.

Our previous study [34] has proved that Ti element keeps negative mixing enthalpy with constituent elements of AlCoCrFeNi system, and the Cu element has the opposite effect. The present investigation was aimed at systematically studying the similarities and differences between the microstructure evolution of AlCoCrFeNiCu alloy and $AlCoCrFeNiTi_{0.5}$ alloy during heat treatment. The results were beneficial for summarizing the influence rules of chemical activity of adding element on the microstructure evolution of AlCoCrFeNi system.

2 Experimental

2.1 Alloy Preparations and Heat Treatments

The ingots with nominal compositions of $AlCoCrFeNiTi_{0.5}$ and AlCoCrFeNiCu were prepared by non-consumable electrode arc-melting in high-purity Ar atmosphere using raw metals with purity higher than 99.9%. To achieve the well mixture in the liquid and improve the chemical homogeneity, the alloys were melted for ~ 40 s with electromagnetic stirring at least four times, and the buttons were flipped between each meting cycle. The melted alloys were eventually suction cast into a water-cooled copper mold to obtain 20 mm × 60 mm × 3 mm plate. In order to systematically study the phase and microstructure transformation process as a function of heating temperature, we performed the following heat treatments: 600 °C, 700 °C, 800 °C, 900 °C, 1000 °C and 1100 °C for 10 h under an Ar-protective environment followed by water quenching.

2.2 Phase Analysis, Microstructural Characterization and Microhardness Determination

Before phase analysis, microstructural characterization and microhardness determination, the samples were abraded on SiC papers up to 4000 grit, and then polished using colloidal silica with size of 0.05 μm. X-ray diffraction (XRD) patterns of the as-cast and heat-treated samples were characterized on a Japan D/max-2400 diffractometer with Cu *K*α radiation operated at 40 kV, 30 mA. The morphology and compositions of the heat-treated samples were examined using a scanning electron microscope (SEM, SUPRA55) equipped with an energy-dispersive spectroscope (EDS) unit. The Vickers microhardness tests were performed using a Duramin-A300 hardness tester under a 500 g load for 15 s. Ten different regions in the sample were selected to test the microhardness and obtain the mean value.

3 Results and Discussion

3.1 $AlCoCrFeNiTi_{0.5}$ Alloy

3.1.1 Phase Transformation of $AlCoCrFeNiTi_{0\cdot5}$ Alloy During Heat Treatment

XRD patterns from $AlCoCrFeNiTi_{0\cdot5}$ alloy in the as-cast condition and after heat treated at different temperatures are presented in Fig. 1a. The pattern from the as-cast $AlCoCrFeNiTi_{0.5}$ alloy contained two BCC peaks. In our previous work [35], the BCC peaks were verified to be an Al–Ni–Ti-rich ordered BCC-B2 and Fe–Cr-rich disordered BCC phase. The ordered BCC-B2 phases shifted to relatively lower angles (to the left) due to the severe lattice distortion by the addition of Ti. The diffraction peaks of B2 and BCC phases showed similar strength. As for $AlCoCrFeNiTi_{0.5}$ alloy, heat treatments caused the following effects: (1) the precipitation of σ phase. The σ phases were precipitated at 700 °C, further multiplied at 800 °C, dissolved at 900 °C and vanished at 1000 °C. The volume fractions of the σ phases were highest at 800 °C. The σ phase maintained a tetragonal structure consisting mostly of Cr and Fe [36]. As shown in Fe–Cr binary alloy phase diagram, the normal precipitation temperature of σ phase in Fe–Cr system is from 545 to 820 °C. Obviously, the precipitation temperature of σ phase went up in the high-entropy alloy. The similar phenomenon has been also observed by Munitz et al. [37]. He found that the σ phase could also precipitate at 850 °C in AlCoCrFeNi high-entropy alloy. The elevated precipitation temperature of σ phase could be attributed to the special structure characters of high-entropy alloy, such as higher lattice distortion, slow diffusion between different elements with a certain difference in atomic radius [38]; (2) the variation in diffraction peak intensity of B2 phase and BCC phase. It could be found that the intensity of B2 and BCC diffraction peaks was significantly influenced by the precipitation and dissolution of σ phase. The intensity of B2 and BCC diffraction peaks drastically decreased at 700 °C, further decreased at 800 °C, whereas increased at 900 °C, and sharply increased at 1000 °C. Namely, the formation and disappearance of the σ phase caused the drastic increase and decrease in diffraction peak intensity of B2 phase and BCC phase, respectively; (3) the shift of the Al–Ni–Ti-rich B2 peaks. As shown in Fig. 1b, the angles of BCC peaks remained constant, while the B2 peaks at 44.00° below 600 °C shifted to 43.88° at 700 °C synchronizing with the precipitation of σ phase. All the phase transformations during heat treatment could be attributed to the diffusion at elevated temperature, which could result in the precipitation of σ phase, composition change and lattice distortion.

3.1.2 Microstructure Evolution of $AlCoCrFeNiTi_{0\cdot5}$ Alloy During Heat Treatment

The impact of heat treatments on the microstructure of $AlCoCrFeNiTi_{0.5}$ alloy as a function of heating temperature is presented in Figs. 2 and 3. The compositions of the different phases as measured by EDS are listed in Table 1. Heating temperatures up to 1100 °C did not affect the dendritic macro-morphology, except for the local micro-morphological change in both dendrites (DR) and interdendritic (ID) regions. The microstructure after heat treating below 600 °C was similar to that in the as-cast condition observed in our previous work [35]. The dendrites core (DC) regions presented dendritic macro-morphology with reticular microstructure textured by ultrafine Fe–Cr-rich BCC structure and Al–Ni–Ti-rich B2 structure. The ID regions consisted of three major phases: the Al–Ni–Ti-rich dark shells (marked as 2 in Fig. 3a) embedded in the Fe–Cr-rich bright matrix

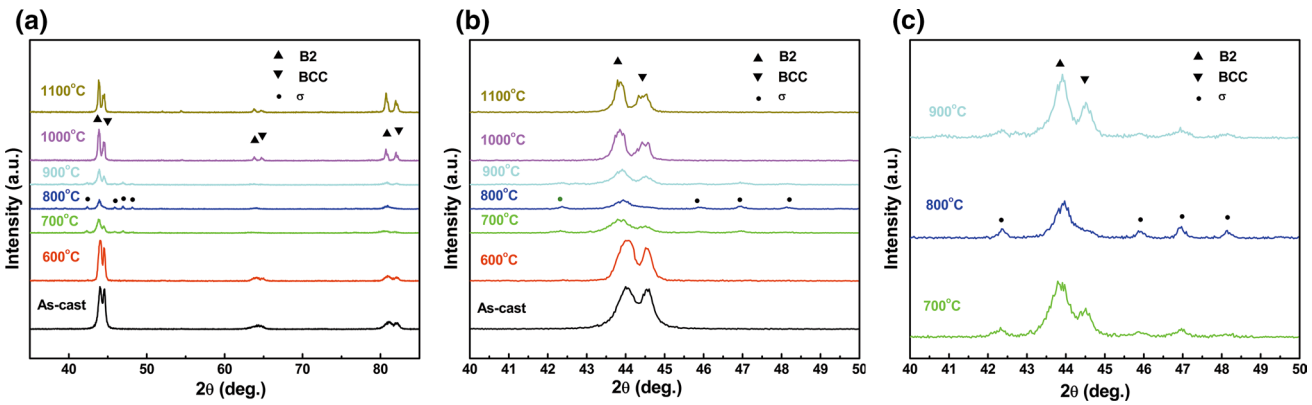

Fig. 1 XRD patterns from the AlCoCrFeNiTi0.5 alloy in the as-cast condition after different heat treatments: **a** whole spectrum; **b**, **c** enlargement of the section between 40° to 50°

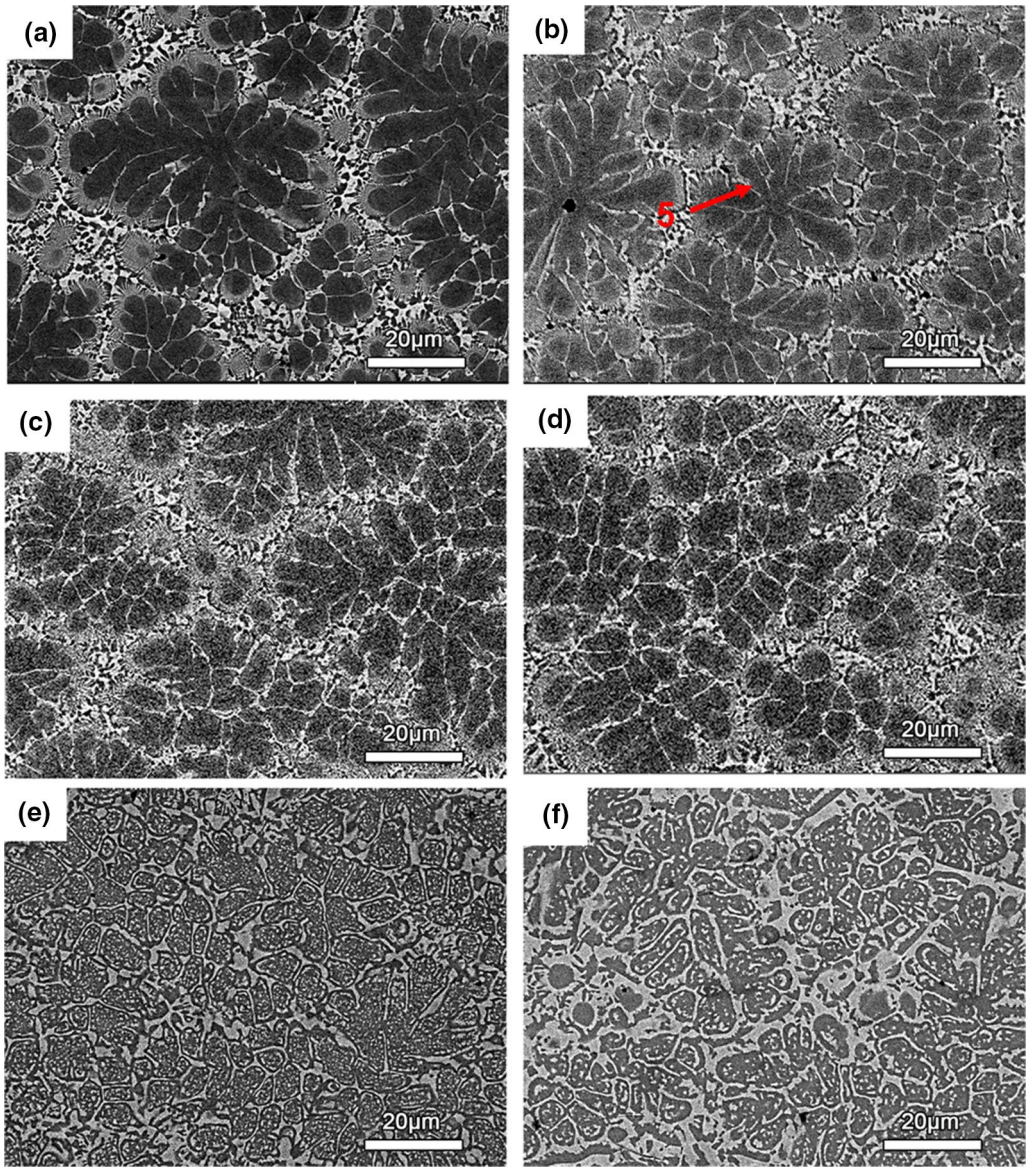

Fig. 2 Backscattered electron images (BEI) at low magnification from the $AlCoCrFeNiTi_{0.5}$ alloy after heat treatments at different temperatures: **a** 600 °C, **b** 700 °C, **c** 800 °C, **d** 900 °C, **e** 1000 °C, **f** 1100 °C

(marked as 1 in Fig. 3a), as well as modulated spinodal-like structure of bright and darker lamellae (marked as 3 in Fig. 3a). In addition, the radiating long alternating lamellar phases (marked as 4 in Fig. 3a) decorated the interface between DC and DR regions.

Heat treatment at 700–900 °C caused the necking and fusing behaviors in the DR regions, as well as the coarsening behaviors in both DC and ID regions. Comparing the micromorphology at different temperatures, it could be found that the Fe–Cr-rich slender necks (marked as 5 in Fig. 2b) began to extend along the branch roots at 700 °C, and the interior of dendrites was completely necked into grains at 900 °C. The needed composition enrichment at the frontier of necking growth interface could come from the special structure of the DC textured by Fe–Cr-rich structure and Al–Ni–Ti-rich structure. Moreover, Fe and Cr elements also kept relatively high solid solubility in Al–Ni–Ti-rich structure due to the high entropy effect [39, 40]. In the ID region, heat treatment at higher temperature promoted the dissolution between different phases, leading to the considerably coarsening of the Fe–Cr-rich white lamellar of both modulated spinodal-like structure in ID (region 3 at 600 °C) and radiating structure in interface (region 4 at 600 °C). The segregated Al–Ni–Ti-rich dark phases surrounded the periphery of the coarsened interface (marked as 7 and 8 in Fig. 3c and d). In addition, the Al–Ni–Ti-rich dark shells embedded in matrix grew

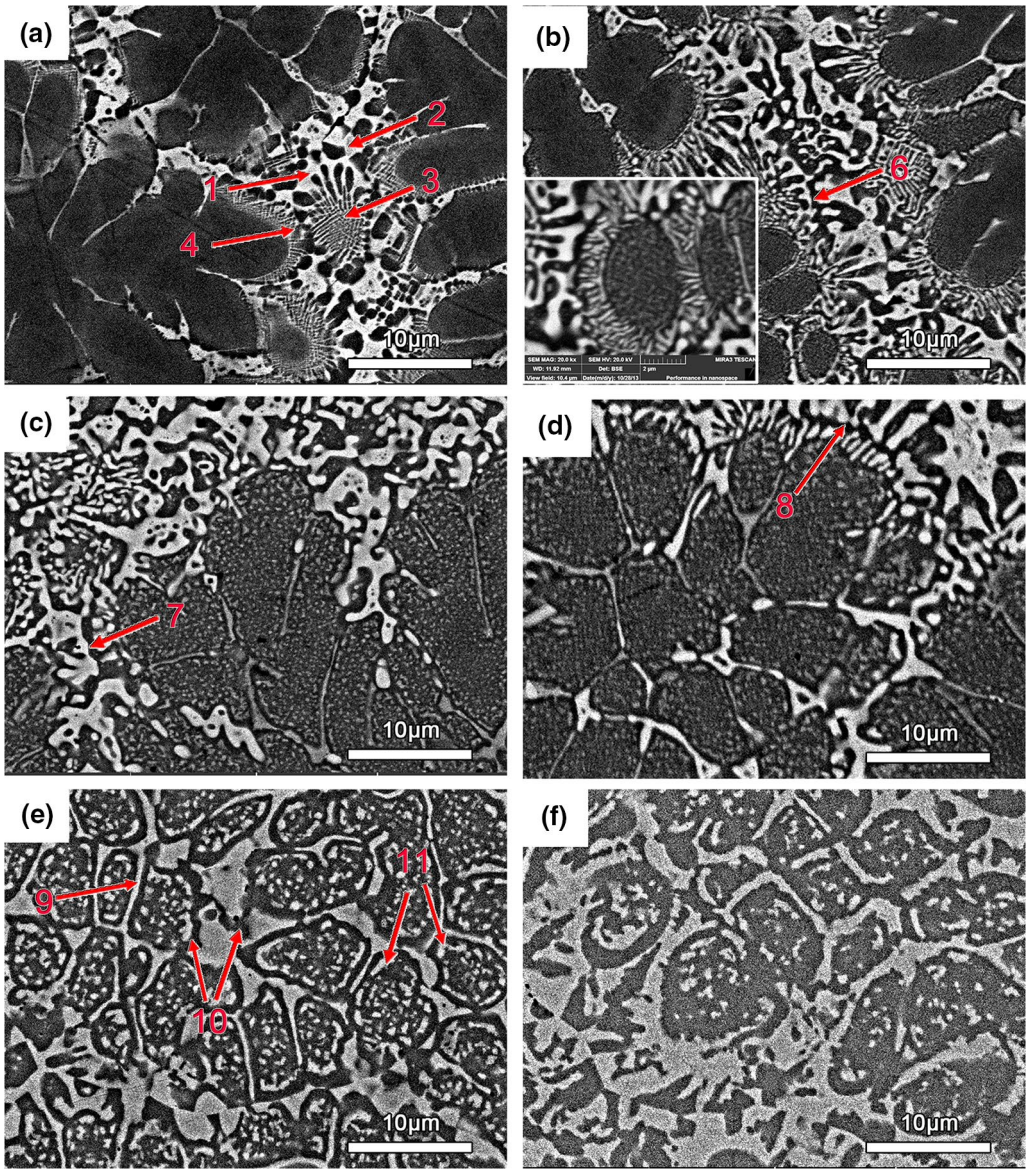

Fig. 3 Backscattered electron images (BEI) at high magnification from the $AlCoCrFeNiTi_{0.5}$ alloy after heat treatments at different temperatures: **a** 600 °C, **b** 700 °C, **c** 800 °C, **d** 900 °C, **e** 1000 °C, **f** 1100 °C

along different orientations, and connected to each other in ID regions (marked as 6 in Fig. 3b). In the DC region, the white cells can be observed in DC at 700 °C, and further coarsened with increasing heating temperature. The white cells are proved to be rich in Fe–Cr in the EDS results of the alloy treated at 1100 °C.

With heat treatments above 1000 °C, the complex phases in ID were replaced by a simple Fe–Cr-rich white block. The boundaries of the grains (marked as 9 in Fig. 3e) were also reinforced. The segregated Al–Ni–Ti-rich dark phases during the coarsening of the Fe–Cr-rich white phases surrounded the periphery of the simple ID region and grain boundaries (marked as 10 in Fig. 3e). In the DC region, the increasing heating temperature further coarsened the Fe–Cr-rich white cells. In addition, coarsened Fe–Cr-rich white cells were inclined to gather along the edge of the grains (marked as 11 in Fig. 3e).

3.1.3 Influence of Heat Treatment on the Hardness of $Alcocrfeniti_{0\cdot5}$ Alloy

The phase transformations and microstructure evolutions of $AlCoCrFeNiTi_{0.5}$ alloy as a function of heating temperature are summarized in Fig. 4. The Vickers microhardness for $AlCoCrFeNiTi_{0\cdot5}$ alloys in the as-cast condition and after different heat treatments is illustrated in Fig. 5.

Table 1 Chemical compositions (in at.%) of different regions of $AlCoCrFeNiTi_{0.5}$ alloys heat treated at different temperatures

Alloy	Region	Al	Co	Cr	Fe	Ni	Ti
	Nominal	18.18	18.18	18.18	18.18	18.18	9.09
600 °C	DC	23.21	17.09	13.23	15.62	20.53	10.32
	ID-Matrix (1)	6.83	17.84	33.16	27.37	10.49	4.31
	ID-Shell (2)	22.71	18.16	13.57	15.71	20.28	9.57
700 °C	DC	22.33	17.71	13.55	15.31	21.13	9.97
	ID-Matrix	7.13	17.91	32.35	27.15	10.89	4.57
	ID-Shell	22.42	18.11	13.47	15.73	20.92	9.35
800 °C	DC	22.91	18.05	14.05	15.42	19.78	9.79
	ID-Matrix	7.85	18.02	30.79	26.93	11.05	5.36
	ID-Shell	22.27	17.46	13.78	15.99	20.54	10.03
900 °C	DC	22.67	18.13	13.25	15.18	20.62	10.15
	ID-Matrix	8.78	17.86	29.13	26.15	12.24	5.84
	ID-Shell	21.95	18.06	10.42	13.39	24.61	11.57
1000 °C	DC-Matrix	20.91	17.75	10.45	13.67	24.38	12.84
	ID	9.63	18.04	27.73	24.92	13.41	6.27
1100 °C	DC-Matrix	20.45	17.34	11.52	14.30	23.95	12.44
	DC-White cells	13.57	18.02	25.76	23.50	16.76	6.39
	ID	10.65	17.81	26.18	24.43	14.57	6.35

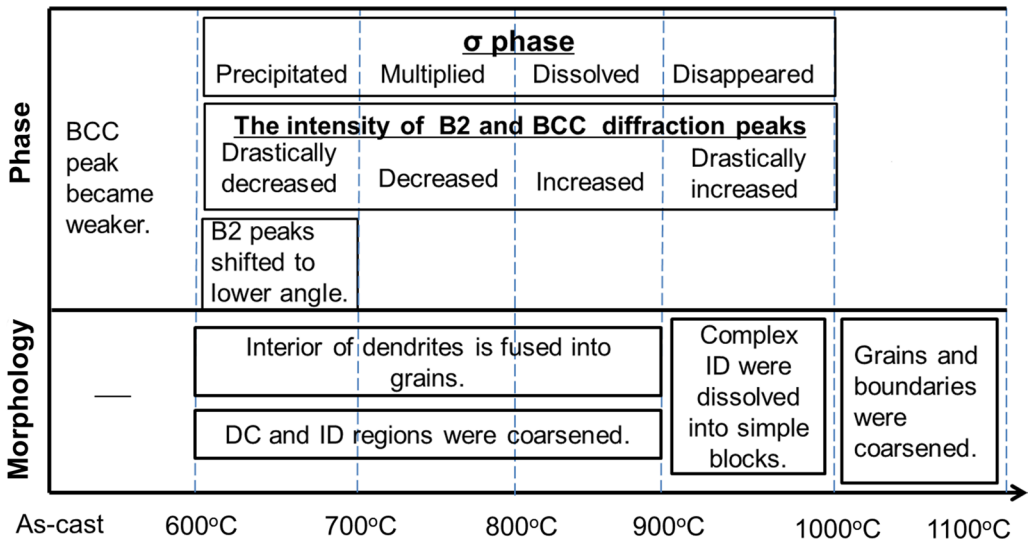

Fig. 4 Rules of phase transformation and morphology evolution of $AlCoCrFeNiTi_{0.5}$ alloy with increasing heating temperatures

As expected, these structural changes have an impact on the mechanical properties. The $AlCoCrFeNiTi_{0.5}$ alloy after heating below 600 °C kept the stable hardness (HV 670). Heating up to 700 °C caused the precipitation of σ phases, the shift of B2 peak to lower angle as well as the intensity decrease in B2 and BCC diffraction peaks. The σ phase with intermetallic compound structure lacked multiple slip systems, and thus was hard and brittle [36]. Both the shifting to lower angle and the intensity decrease in diffraction peaks meant the aggravation of the lattice distortion [41, 42]. The dispersion strengthening and the reinforced solution strengthening enhanced the hardness to HV 704. With the following change in the amount of σ phases and the lattice distortion of BCC phases, the hardness further increased to HV 745 after heating at 800 °C, contrarily decreased to HV 693 and HV 610 after heating at 900 °C and 1000 °C. Heat treatment at 1100 °C caused pronounced coarsening in grains and boundaries, leading to the further reduction in hardness (to HV 560).

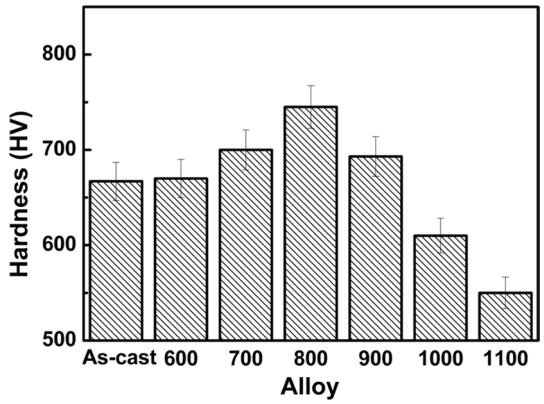

Fig. 5 Vickers hardness for $AlCoCrFeNiTi_{0.5}$ alloy in the as-cast condition and after different heat treatments

3.2 AlCoCrFeNiCu Alloy

3.2.1 Phase Transformation of AlCoCrFeNiCu Alloy During Heat Treatment

XRD patterns of the as-cast and heat-treated AlCoCrFeNiCu alloys are presented in Fig. 6. The pattern from the as-cast alloy contained large BCC peaks with smaller amount of an FCC phase. It has been proved that the BCC diffraction peaks in AlCoCrFeNiCu alloy actually contained Fe–Cr-rich BCC phase and Al–Ni-rich B2 phase [43]. Due to the identical lattice parameters, diffraction peaks of BCC phase and B2 phase coincided with each other, and were not able to be conspicuously distinguished by the XRD [35]. The FCC phase in the as-cast condition was rich in Cu. As for AlCoCrFeNiCu alloy, heat treatment caused the following effects: (1) the transformation of FCC phase from initial Cu-rich FCC1 phase to FCC2 phase. In the as-cast and heat-treated below 600 °C conditions, there was a single Cu-rich FCC1 phase. Heating at 700 °C, the second FCC phase (FCC2) with larger angles compared with the initial Cu-rich FCC1 phase was nucleated, the single FCC1 peaks split into FCC1 peaks and FCC2 peaks. The initial Cu-rich FCC1 phase was dissolved at heating temperature above 1000 °C, and vanished after heating at 1100 °C. Single FCC2 peaks could be observed after heating at 1100 °C; (2) the variation in diffraction peak intensity of B2 phase and BCC phase. The diffraction peaks intensity of B2 phase and BCC phase decreased from the as-cast condition to heat-treated condition up to 900 °C, then contrarily increased when the temperature increased above 1000 °C. The transformation in FCC phases and the dissolution of FCC 1 phase could affect the diffraction peak intensity of B2 phase and BCC phase; (3) the shifting to lower angle of the FCC1 and FCC2 peaks. After the splitting of FCC phases, both the diffraction peaks of FCC1 phase and FCC2 phase gradually shifted to lower angle with the temperature increasing from 700 to 1100 °C.

3.2.2 Microstructure Evolution of AlCoCrFeNiCu Alloy During Heat Treatment

The impact of heat treatments on the microstructure of AlCoCrFeNiCu alloy as a function of heating temperature is presented in Figs. 7 and 8. The compositions of the different phases as measured by EDS are listed in Table 2. Heating temperatures up to 900 °C did not affect the dendritic macro-morphology. In contrast, heat treatment above 1000 °C caused the prominent dissolution between different phases, as well as the dramatic change in macro-morphology. The microstructure after heat treating below 600 °C was similar to that in the as-cast condition observed in our previous work [35]. The DC region consisted of reticular structure and some Cu-rich FCC precipitated. The reticular structure was textured by the Fe–Cr-rich BCC structure and Al–Ni-rich B2 structure [43]. Different from the complex ID structure

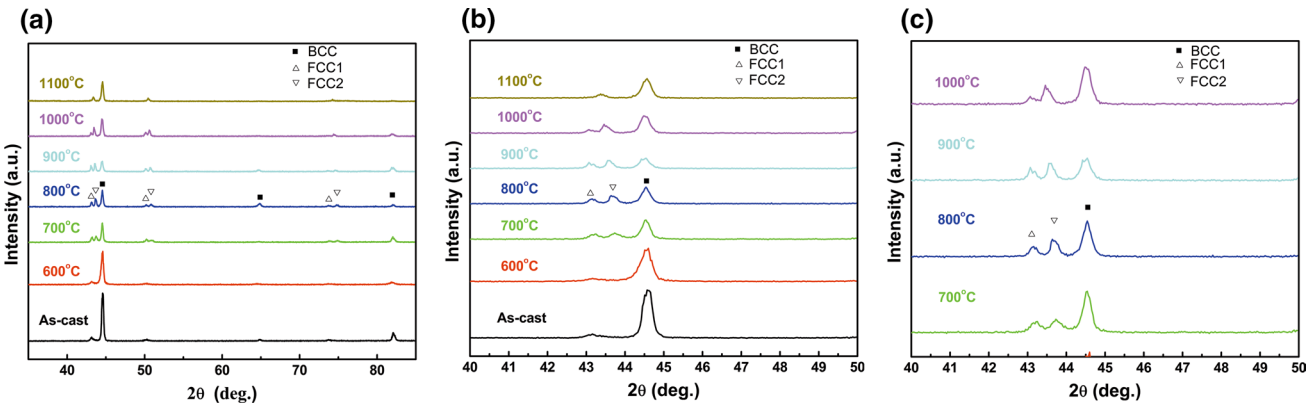

Fig. 6 XRD patterns from the AlCoCrFeNiCu alloy in the as-cast condition after different heat treatments: **a** whole spectrum; **b**, **c** enlargement of the section between 40° to 50°

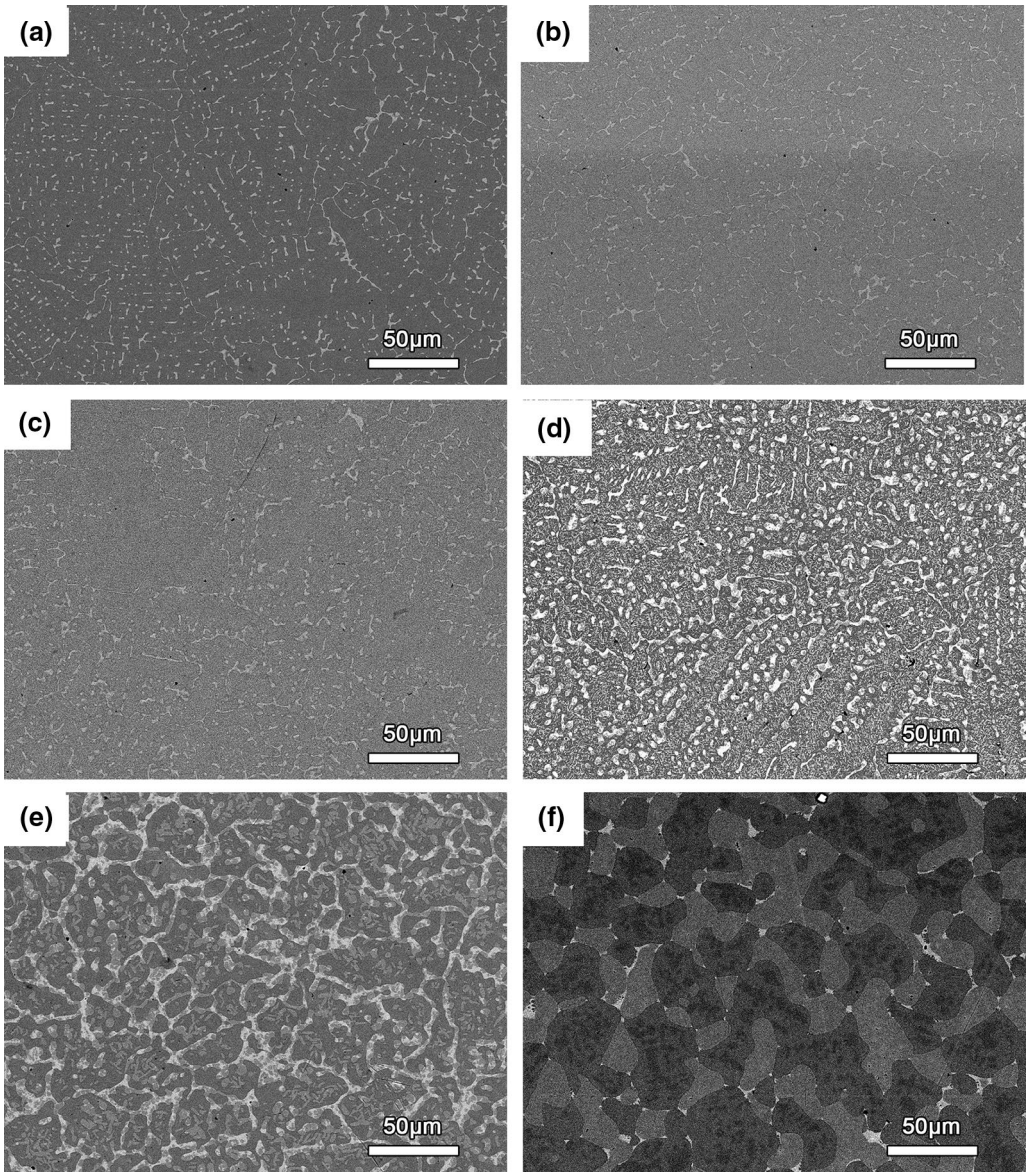

Fig. 7 Backscattered electron images (BEI) at low magnification from the AlCoCrFeNiCu alloy after heat treatments at different temperatures: **a** 600 °C, **b** 700 °C, **c** 800 °C, **d** 900 °C, **e** 1000 °C, **f** 1100 °C

of $AlCoCrFeNiTi_{0.5}$ alloy, the ID region of AlCoCrFeNiCu alloy maintained simple Cu-rich FCC phase with thin and long morphologies. The formation of the simple Cu-rich ID could be put down to the strong repulsive interaction between Cu and the other elements [44].

Heating at 700–900 °C mainly caused phase coarsening in both DC and ID regions as well as the formation of Cu–Al–Ni-rich FCC2 phase in ID region. In the DC regions, the Al–Ni-rich gray rod-like phases embedded in Fe–Cr-rich black matrix (marked as 1 in Fig. 8d) could be observed at 700 °C, and further coarsened with increasing heating temperature. The Al–Ni-rich phase contained more Cu element (~ 13 at.%) than the Fe–Cr-rich matrix phase (~ 7 at.%) at 900 °C, which can be attributed to the negligible mutual solubility between Cu and Cr (solid solubility of Cr in Cu is 0.65 at.% in the equilibrium state) [45]. In the ID regions, the heat treatment also caused the coarsening of Cu-rich ID regions, especially when the heating temperature increased from 800 to 900 °C. At the same time, some Cu–Al–Ni-rich gray grains (marked as 3 in Fig. 8d) emerged in the white matrix of ID, and multiplied with increasing heating temperature. The gray grains showed considerably lower Cu contents (~ 25 at.%) than the white matrix(~ 60 at.%), obviously corresponding to the FCC2 peaks in the XRD patterns. The coarse white matrix (marked as 2 in Fig. 9d) of the ID at 900 °C owned

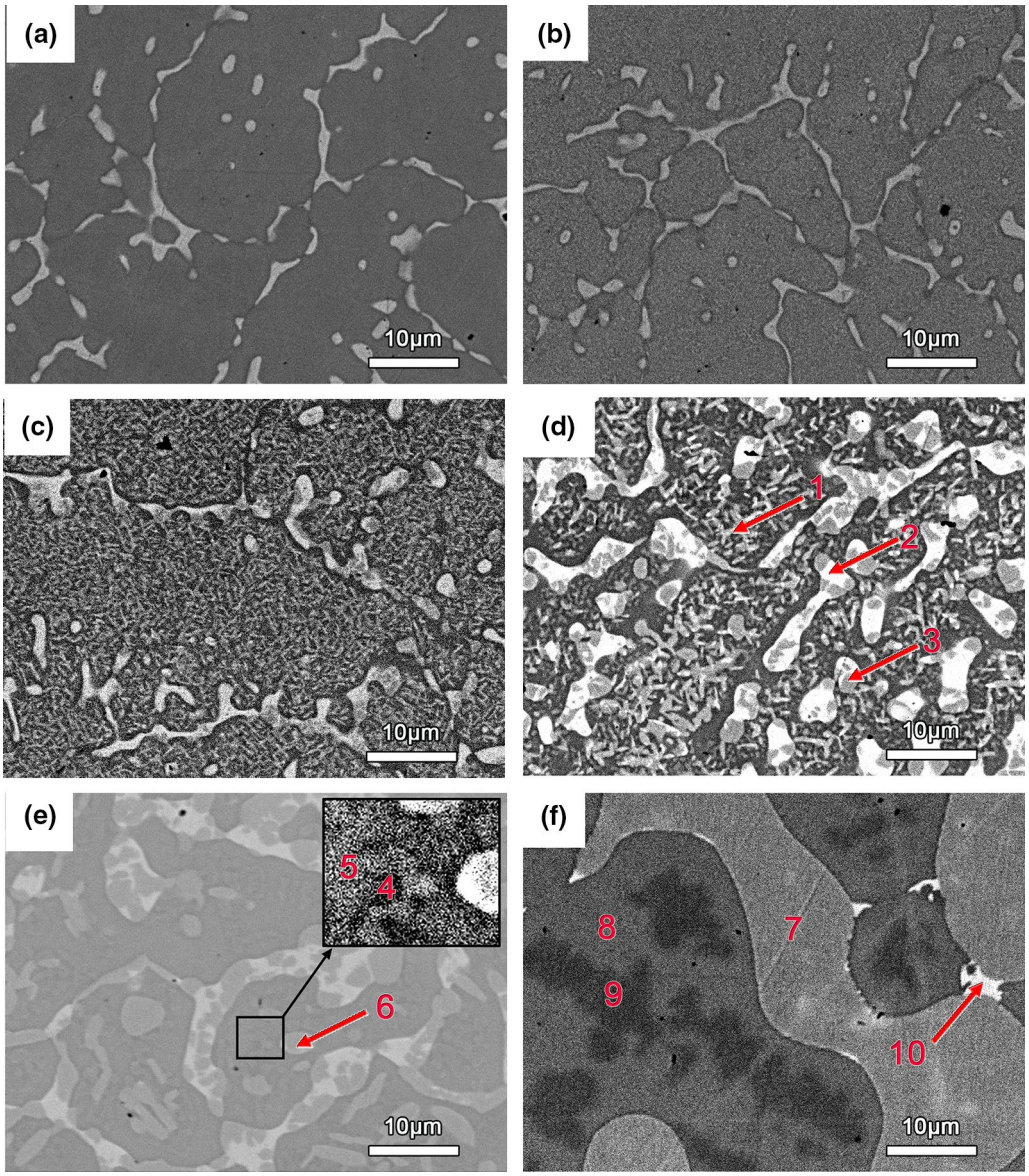

Fig. 8 Backscattered electron images (BEI) at high magnification from the AlCoCrFeNiCu alloy after heat treatments at different temperatures: **a** 600 °C, **b** 700 °C, **c** 800 °C, **d** 900 °C, **e** 1000 °C, **f** 1100 °C

the similar Cu content (~ 60 at.%) with the thin ID region at 600 °C. The formation and multiplication of Cu–Al–Ni-rich gray grains were responsible for the coarsening behaviors of the Cu-rich ID region.

Upon heating to 1000 °C, a dramatic change took place. The further coarsened ID regions connected to each other, transforming the macrostructure from dendritic morphology to equiaxed morphology. The amount of the Cu–Al–Ni-rich FCC2 phase in ID further increased, while the Cu content of the ID-matrix decreased to ~ 43 at.%. In the DC regions, the heat treatment caused the further coarsening (marked as 4 and 5 in Fig. 8e), and the emergence of Cu–Al–Ni-rich gray grains (marked as 6 in Fig. 8e).

Additional dramatic changes occurred after heat treatment at 1100 °C, where the microstructure became much coarser. All the complex phases in ID and DC of AlCoCrFeNiCu alloy were replaced by four phases: (1) the brighter gray matrix which was Cu–Al–Ni-rich FCC2 phases (marked as 7 in Fig. 8f), (2) darker gray matrix which was Al–Ni-rich B2 phases (marked as 8 in Fig. 8f), (3) the dark phases which were Fe–Cr-rich BCC structure with block or dendritic morphologies (marked as 9 in Fig. 8f) embedded in the "8" darker gray matrix, (4) a low volume of Cu-rich phases (marked as 10 in Fig. 8f) dispersing in the interface between "7" Cu–Al–Ni-rich matrix and "8" Al–Ni-rich matrix. The Cu–Al–Ni-rich brighter gray matrix at 1100 °C showed the

Table 2 Chemical compositions (in at.%) of different regions of AlCoCrFeNiCu alloys heat treated at different temperatures

Alloy	Region	Al	Co	Cr	Fe	Ni	Cu
	Nominal	16.66	16.66	16.66	16.66	16.66	16.66
600	DC	15.69	18.17	18.83	18.55	14.99	12.76
	ID	11.09	5.51	4.27	5.59	10.44	63.09
700	DC	14.65	17.93	21.02	21.39	14.61	10.41
	ID	10.60	6.52	4.37	6.18	10.06	58.63
800	DC	14.15	18.98	19.01	19.66	15.47	12.73
	ID-Matrix	10.85	7.37	4.39	6.53	10.73	60.14
900	DC-Matrix	10.41	18.92	24.91	24.31	13.26	7.18
	DC-Precipitate(1)	20.81	17.49	13.47	14.01	21.87	12.35
	ID-Matrix (2)	8.78	8.14	6.99	7.77	9.01	58.31
	ID-Precipitate(3)	19.99	11.73	10.82	12.03	20.23	25.21
1000	DC-Matrix	15.06	19.95	20.15	19.72	15.84	9.28
	DC-Precipitate(6)	20.20	14.55	10.96	12.31	20.81	20.17
	ID-Matrix	11.59	11.40	11.88	11.74	10.45	42.93
	ID-Precipitate	20.14	12.39	10.04	11.73	20.90	24.80
1100	Matrix-7	19.25	11.98	9.65	10.70	24.51	23.90
	Matrix-8	21.08	17.19	16.12	16.23	20.34	9.04
	Precipitate-9	7.42	18.10	30.26	28.59	10.01	5.63
	Precipitate-10	6.21	6.80	4.30	7.27	7.28	68.14

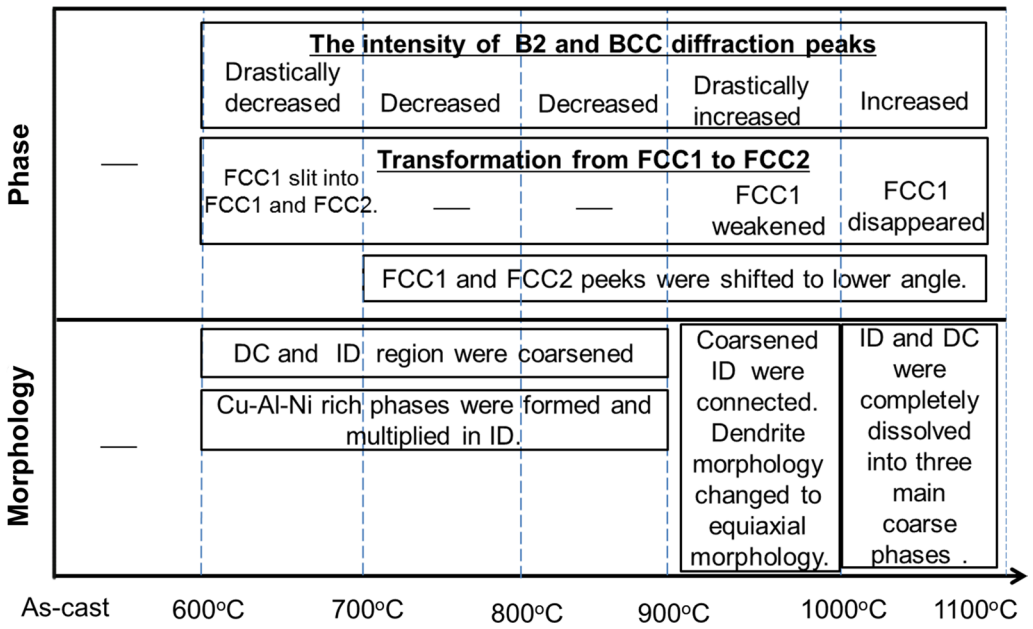

Fig. 9 Rules of phase transformation and morphology evolution of AlCoCrFeNiCu alloy with increasing heating temperatures

similar compositions to the gray phases formed and multiplied in the Cu-rich ID region from 700 to 1000 °C. In addition, the Cu content of the matrix of Cu-rich ID at 900 °C (region "2"), the matrix of grain boundary at 1000 °C and coarse phases at 1100 °C (region "7") were about ~ 60 at.%, ~ 43 at.% and ~ 25 at.%, respectively. It can be inferred that the Cu–Al–Ni-rich FCC2 phases with lower Cu content were more stable than the Cu-rich FCC1 phase. During solidification, the Cu-rich FCC1 phases were segregated due to the preferential formation of Al–Ni and Fe–Cr phases. While heating above 700 °C, more stable Cu–Al–Ni-rich FCC2 phases tended to nucleate in the segregated Cu-rich FCC1 region. Upon heating to 1100 °C, most Cu-rich FCC1 phases were transformed into Cu–Al–Ni-rich FCC2 phases.

The residual Cu-rich FCC1 phases became undetected in the XRD patterns because of their low volume fractions and dimensions.

3.2.3 Influence of Heat Treatment on the Hardness of AlCoCrFeNiCu Alloy

The phase transformations and microstructure evolutions of AlCoCrFeNiCu alloy as a function of heating temperature are summarized in Fig. 9. The Vickers microhardness for AlCoCrFeNiCu alloys in the as-cast condition and after different heat treatments is illustrated in Fig. 10. There are several factors influencing the mechanical properties obtained from microhardness testing. The aggravated lattice distortion of BCC phase and FCC phases, as confirmed by the intensity decrease in the BCC diffraction peaks and the shift of FCC diffraction peaks to lower angle (in Fig. 7), could strengthen the alloy. However, the coarsening of the DC and the extension of FCC phase due to the transformation from FCC1 to FCC2 phase, as confirmed by the morphology evolution (in Figs. 7, 8), could reduce the hardness. With the similar structure, the AlCoCrFeNiCu alloy kept stable hardness (HV 481) below 600 °C. Heating up to 700 °C and 800 °C, the transformation from Cu-rich FCC1 phases to Cu–Al–Ni-rich FCC2 phases in ID, as well as the coarsening DC regions, resulted in the reduction in hardness (HV 453 and HV 445).

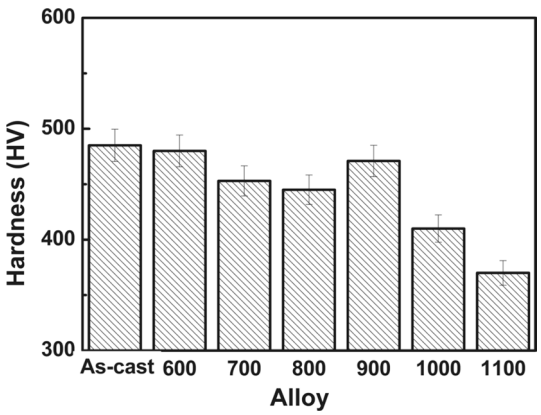

Fig. 10 Vickers hardness for AlCoCrFeNiCu alloy in the as-cast condition after different heat treatments

Heating at 900 °C abnormally increased the hardness to HV 471, which was ascribed to the aggravated lattice distortion of BCC phase and FCC phase. When the heating temperature increased above 1000 °C, the pronounced coarsening of the microstructure and larger volume fraction of FCC phase led to the sharp reduction in hardness (HV 410 and HV 370).

3.3 Impact of Ti Element and Cu Element on the Phase Transformation and Microstructure Evolution

As described above, adding Ti and Cu within certain contents still kept the solid solution structure of HEAs, which could be attributed to the high mixing entropy and rapid cooling rate during unequilibrium solidification. On the other side, additives with different physical and chemical characteristics (such as mixing enthalpies with constituent elements, atomic radius) [46], as listed in Table 3, have different impacts on the microstructure and mechanical properties of the AlCoCrFeNi systems.

Additives owning negative mixing enthalpies with constituent elements could trigger reactions. Most of these additives reacted with certain element owning larger mixing enthalpy, and the residuals would be dissolved in the phases containing elements owning lower mixing enthalpy. Ti with the largest mixing enthalpies with Ni (− 35 kJ/mol) was mainly aggregated in the Al–Ni-rich B2 phases, partly dissolved in the Fe–Cr-rich BCC phase. The reaction and dissolution of additives could aggravate the lattice distortion and affect the precipitation during heat treatment. Due to the larger atomic radius of Ti, the formed Al–Ni–Ti-rich phases aggravated the lattice distortion of B2 phases, and enhanced the solid solution strengthening and the hardness (HV 670). Zhang et al. have also found that $AlCoCrFeNiTi_{0.5}$ alloy with effective multiple strengthening mechanisms, such as solid solution strengthening, precipitating strengthening and nano-composite strengthening effects, could exhibit higher yield strength and fracture strength than AlCoCrFeNi alloy [47]. However, adding more Ti element could lead to the decrease in the strength and plasticity [25], which might be due to the simultaneously caused morphologic transformation. Previous work has proved that Fe–Cr–Co–Ni-rich FCC phases could emerge in AlCoCrFeNi alloy during

Table 3 Atom size (Å) and the mixing enthalpy (kJ/mol) of different elements

Element (atomic radius)	Al(1.82)	Co(1.67)	Cr(1.85)	Fe(1.72)	Ni(1.62)	Ti(2.00)	Cu(1.57)
Al		− 19	− 10	− 11	− 22	− 30	− 1
Co			− 4	− 1	0	− 28	6
Cr				− 1	− 7	− 7	12
Fe					− 2	− 17	13
Ni						− 35	4

heating above 850 °C [37]. The addition of Ti element inhibited the formation of FCC phases during heat treatment. It has also been found that the FCC phases could form in the as-cast $AlCoCrFeNiCu_{0.5}$ alloy [48]; however, there were no obvious FCC phases observed in the as-cast $AlCoCrFeNiCu_{0.5}Ti_{0.5}$ alloy [49]. In addition, the structure alteration in Fe–Cr-rich phases by dissolving Ti enhanced the precipitation of Fe–Cr-rich σ phase from 700 to 900 °C. The precipitation and disappearance of σ phase could affect the lattice distortion of B2 and BCC phases. Variations in σ phase amount and lattice distortion dominated the hardness change in $AlCoCrFeNiTi_{0.5}$ alloy during heat treatment. The dissolution of additive also could enhance the slow diffusion and thermal stability of high-entropy alloy. The $AlCoCrFeNiTi_{0.5}$ alloy maintained the dendritic morphology even upon heating at 1100 °C.

Additives owning positive mixing enthalpies with constituent elements tend to form segregation. Due to the miscibility between additives and constitute elements, the segregated phase was inclined to undergo transformation during heat treatment. Cu tended to be repelled to the ID region during solidification. Al and Ni could be dissolved in Cu-rich phases. The Cu-rich FCC1 phases were inclined to transform into Cu–Al–Ni-rich FCC2 phases when the temperature was satisfied. The addition of Cu not only resulted in the formation of FCC phases, but also reduced the volume fraction of Al–Ni-rich intermetallic in DC, thus decreasing the hardness (HV 481). The transformation in the segregated phase could inhibit the precipitation of σ phase and reduce the microstructure stability. Munitz et al. have found that the σ phase could appear in $Al_{1.25}CoCrFeNiCu$ alloy after heat treated at 650 °C [50]. It seems that the additives owning negative mixing enthalpies with constituent elements and larger atomic radius (such as Ti, Al) could promote the precipitation of σ phase, and the additives owning positive mixing enthalpy with constituent elements (such as Cu) would give the opposite effect. As the Cu–Al–Ni-rich FCC2 phase contained less Cu contents than Cu-rich FCC1, the FCC regions extended in the morphology accompanied with the transformation from FCC1 to FCC2 for the alloy with constant Cu content. The AlCoCrFeNiCu alloy suffered dramatic changes in the morphologies above 1000 °C. The increased volume fraction of FCC phases and the dramatic coarsening of the microstructure dominated the hardness change in AlCoCrFeNiCu alloy during heat treatment.

In addition, additives with different chemical activities could affect the phase proportion and coarsening behavior during heat treatment in DC region. In $AlCoCrFeNiTi_{0.5}$ alloy, adding Ti increased the phase proportion of Al–Ni–Ti-rich phases in DC. The Fe–Cr-rich bright lamellae embedded in the Al–Ni–Ti-rich dark matrix and coarsened to cellular morphology with increasing heating temperature. In AlCoCrFeNiCu alloy, the segregated Cu-rich ID region exhibited some solubility for Al and Ni. With higher content of Fe–Cr-rich phases in DC, the Al–Ni-rich bright lamellae embedded in the Fe–Cr-rich dark matrix and coarsened to rod-like morphology with increasing heating temperature.

It has been proved that the toughness and micro-crack behaviors of AlCoCrFeNi systems could be ameliorated by optimizing microstructure [51-54]. With inter-woven short rods and nano-particles distributed in matrix, the $Al_{0.5}CrFeNiTi_{0.25}$ alloy showed the fracture strain of 40% [51]. The formation of Cu-rich FCC solid solution phase and transformation-induced FCC solid solution phase resulted in 36.69% plasticity of $AlCoCrFeNiCu_{2.0}$ alloy [48]. Due to the capability of nano-twinning as well as ductile dimple fracture affected by the microstructure characteristic, the $Al_{0.3}CoCrFeNi$ alloy showed higher strain at 298 K but lower higher strain at 77 K than $Al_{0.1}CoCrFeNi$ alloy [52]. On account of the fine FCC structure strengthened by dense NiAl-type B2 precipitation, annealing at 900 °C increased the elongation of $Al_{0.3}CoCrFeNi$ alloy fibers from 8 to 25% [53, 54]. It is believed that the structure optimization through the addition of Ti and Cu followed by heat treatment could effectively improve the toughness and ameliorate the micro-cracking in AlCoCrFeNi system. The relationship between microstructure evolution and micro-cracking behavior in AlCoCrFeNi system would be investigated in our future work.

4 Conclusions

1. Adding Ti with high chemical activity aggravated the lattice distortion of Al–Ni B2 phases, promoted the formation of σ phase from 700 to 900 °C, and inhibited the formation of FCC phases during heat treatment.
2. Adding Cu with low chemical activity generated the metastable Cu-rich FCC1 phases and inhibited the formation of σ phase during heat treatment. The Cu-rich FCC1 phases transformed into Cu–Al–Ni-rich FCC2 phases with increasing temperature, extending the volume fraction of the FCC phase in the morphology.
3. The lattice distortion of B2 and BCC phases in both $AlCoCrFeNiTi_{0.5}$ alloy and AlCoCrFeNiCu alloy was first intensified and then relieved with increasing temperature. The formation and disappearance of σ phase, Cu–Al–Ni-rich FCC2 phase and Cu-rich FCC1 phase could lead to the drastic variation in lattice distortion of the B2 and BCC phases.
4. Adding Ti made the stable dendritic micro-morphology and complex ID structure, while adding Cu made the unstable dendritic micro-morphology and simple ID structure. AlCoCrFeNiCu alloy suffered two dramatic changes in the morphologies at 1000 °C and 1100 °C.

5. The variation in lattice distortion of B2 and BCC phases as well as the precipitation and dissolution of σ phase resulted in that the hardness of $AlCoCrFeNiTi_{0.5}$ alloy increased from room temperature to 800 °C, then decreased as the temperature further increased. The increasing volume fraction of FCC phases and coarsening behaviors in the morphologies generated that the hardness of the AlCoCrFeNiCu alloy mainly decreased with increasing heating temperature, apart from the sudden increase at 900 °C.

Acknowledgements This work was financially supported by the National Key R&D Program of China (No. 2018YFB2000100) and the National Natural Science Foundation of China (Nos. 51701227 and 51775532); one of the authors (Zhuhui Qiao) appreciates the support of the Taishan scholars Program of Shandong Province and the Outstanding Talents of Qingdao Innovations.

References

[1] Z. Li, S. Zhao, R.O. Ritchie, M.A. Meyers, Prog. Mater. Sci. **102**, 296 (2019)
[2] Y.F. Ye, Q. Wang, J. Lu, C.T. Liu, Y. Yang, Mater. Today **19**, 349 (2016)
[3] H. Zhang, B. Dou, H. Tang, Y. He, S. Guo, Mater. Des. **159**, 224 (2018)
[4] Y.L. Zhang, J.G. Li, X.G. Wang, Y.P. Lu, Y.Z. Zhou, X.F. Sun, J. Mater. Sci. Technol. **35**, 902 (2019)
[5] Y.P. Lu, H.F. Huang, X.Z. Gao, C.L. Ren, J. Gaob, H.Z. Zhang, S.J. Zheng, Q.Q. Jin, Y.H. Zhao, C.Y. Lu, T.M. Wang, T.J. Li, J. Mater. Sci. Technol. **35**, 369 (2019)
[6] C. Xiang, Z.M. Zhang, H.M. Fu, E.H. Han, J.Q. Wang, H.F. Zhang, G.D. Hu, Acta Metall. Sin. (Engl. Lett.) **32**, 1053 (2019)
[7] M.H. Tsai, J.W. Yeh, Mater. Res. Lett. **2**, 107 (2014)
[8] S. Chen, K.K. Tseng, Y. Tong, W. Li, C.W. Tsai, J.W. Yeh, P.K. Liaw, J. Alloy. Compd. **795**, 19 (2019)
[9] Y. Zhang, T.T. Zuo, Z. Tang, M.C. Gao, K.A. Dahmen, P.K. Liaw, Z.P. Lu, Prog. Mater. Sci. **61**, 1 (2014)
[10] T.T. Zuo, M.C. Gao, L.Z. Ouyang, X. Yang, Y.Q. Cheng, R. Feng, S.Y. Chen, P.K. Liaw, J.A. Hawk, Y. Zhang, Acta Mater. **130**, 10 (2017)
[11] Y.P. Lu, H. Jiang, S. Guo, T.M. Wang, Z.Q. Cao, T.J. Li, Intermetallics **91**, 124 (2017)
[12] L. Jiang, Y.P. Lu, M. Song, C. Lu, K. Sun, Z.Q. Cao, T.M. Wang, F. Gao, L.M. Wang, Scr. Mater. **165**, 128 (2019)
[13] D.X. Qiao, H. Jiang, W.N. Jiao, Y.P. Lu, Z.Q. Cao, T.J. Li, Acta Metall. Sin. (Engl. Lett.) **32**, 925 (2019)
[14] J.B. Cheng, D. Liu, X.B. Liang, B.S. Xu, Acta Metall. Sin. Engl. Lett. **27**, 1031 (2014)
[15] L.M. Du, L.W. Lan, S. Zhu, H.J. Yang, X.H. Shi, P.K. Liaw, J.W. Qiao, J. Mater. Sci. Technol. **35**, 917 (2019)
[16] Y. Yu, J. Wang, J.S. Li, J. Yang, H.C. Kou, W.M. Liu, J. Mater. Sci. Technol. **32**, 470 (2016)
[17] E.P. George, D. Raabe, R.O. Ritchie, Nat. Rev. Mater. **4**, 515 (2019)
[18] Z.M. Li, K.G. Pradeep, Y. Deng, D. Raabe, C.C. Tasan, Nature **534**, 227 (2016)
[19] B. Gludovatz, A. Hohenwarter, D. Catoor, E.H. Chang, E.P. George, R.O. Ritchie, Science **345**, 1153 (2014)
[20] Y.P. Lu, Y. Dong, S. Guo, L. Jiang, H.J. Kang, T.M. Wang, B. Wen, Z.J. Wang, J.C. Jie, Z.Q. Cao, H.H. Ruan, T.J. Li, Sci. Rep. **4**, 5 (2014)
[21] Y. Lu, X. Gao, L. Jiang, Z. Chen, T. Wang, J. Jie, H. Kang, Y. Zhang, S. Guo, H. Ruan, Y. Zhao, Z. Cao, T. Li, Acta Mater. **124**, 143 (2017)
[22] X.Z. Gao, Y.P. Lu, B. Zhang, N.N. Liang, G.Z. Wu, G. Sha, J.Z. Liu, Y.H. Zhao, Acta Mater. **141**, 59 (2017)
[23] Y.P. Lu, X.X. Gao, Y. Dong, T.M. Wang, H.L. Chen, H.H. Mao, Y.H. Zhao, H. Jiang, Z.Q. Cao, T.J. Li, S. Guo, Nanoscale **10**, 1912 (2018)
[24] J. Hou, X. Shi, J. Qiao, Y. Zhang, P.K. Liaw, Y. Wu, Mater. Des. **180**, 107910 (2019)
[25] Y.J. Zhou, Y. Zhang, Y.L. Wang, G.L. Chen, Appl. Phys. Lett. **90**, 18 (2007)
[26] C.J. Tong, M.R. Chen, S.K. Chen, J.W. Yeh, T.T. Shun, S.J. Lin, S.Y. Chang, Metall. Mater. Trans. A-Phys. Metall. Mater. Sci. **36a**, 1263 (2005)
[27] Z.J.W.X.L. Shang, Q.F. Wu, J.C. Wang, J.J. Li, J.K. Yu, Acta Metall. Sin. (Engl. Lett.) **32**, 41 (2019)
[28] Y.T. Wang, J.B. Li, Y.C. Xin, X.H. Chen, M. Rashad, B. Liu, Y. Liu, Acta Metall. Sin. (Engl. Lett.) **32**, 932 (2019)
[29] T.D. Huang, H. Jiang, Y.P. Lu, T.M. Wang, T.J. Li, Appl. Phys. A-Mater. **125**, 180 (2019)
[30] A. Munitz, S. Salhov, G. Guttmann, N. Derimow, M. Nahmany, Mater. Sci. Eng. A **742**, 1 (2019)
[31] J.C. Rao, H.Y. Diao, V. Ocelik, D. Vainchtein, C. Zhang, C. Kuo, Z. Tang, W. Guo, J.D. Poplawsky, Y. Zhou, P.K. Liaw, J.T.M. De Hosson, Acta Mater. **131**, 206 (2017)
[32] A. Verma, P. Tarate, A.C. Abhyankar, M.R. Mohape, D.S. Gowtam, V.P. Deshmukh, T. Shanmugasundaram, Scr. Mater. **161**, 28 (2019)
[33] Z.W. Yuan, W.B. Tian, F.G. Li, Q.Q. Fu, Y.B. Hu, X.G. Wang, J. Alloy. Compd. **806**, 901 (2019)
[34] Y. Yu, J. Wang, J. Yang, Z.H. Qiao, H.T. Duan, J.S. Li, J. Li, W.M. Liu, Tribol. Int. **131**, 24 (2019)
[35] Y. Yu, J. Wang, J.S. Li, H.C. Kou, W.M. Liu, Mater. Lett. **138**, 78 (2015)
[36] M. Chen, L. Lan, X.H. Shi, H.J. Yang, M. Zhang, J.W. Qiao, J. Alloy. Compd. **777**, 180 (2019)
[37] A. Munitz, S. Salhov, S. Hayun, N. Frage, J. Alloy. Compd. **683**, 221 (2016)
[38] K.Y. Tsai, M.H. Tsai, J.W. Yeh, Acta Mater. **61**, 4487 (2013)
[39] A. Karati, M. Nagini, S. Ghosh, R. Shabadi, K.G. Pradeep, R.C. Mallik, B.S. Murty, U.V. Varadaraju, Sci. Rep. **9**, 5331 (2019)
[40] B.S. Murty, J.W. Yeh, S. Ranganathan, *High Entropy Alloys*, 1st edn. (Butterworth-Heinemann, Boston, 2014)
[41] F.J. Wang, Y. Zhang, G.L. Chen, J. Alloy. Compd. **478**, 321 (2009)
[42] C. Lee, G. Song, M.C. Gao, R. Feng, P. Chen, J. Brechtl, Y. Chen, K. An, W. Guo, J.D. Poplawsky, S. Li, A.T. Samaei, W. Chen, A. Hu, H. Choo, P.K. Liaw, Acta Mater. **160**, 158 (2018)
[43] S. Singh, N. Wanderka, B.S. Murty, U. Glatzel, J. Banhart, Acta Mater. **59**, 182 (2011)
[44] A. Munitz, M.J. Kaufman, M. Nahmany, N. Derimow, R. Abbaschian, Mater. Sci. Eng. A **714**, 146 (2018)
[45] D.Y. Shih, C.A. Chang, J. Paraszczak, S. Nunes, J. Cataldo, J. Appl. Phys. **70**, 3052 (1991)
[46] A. Takeuchi, A. Inoue, Mater. Trans. **46**, 2817 (2005)
[47] Y.J. Zhou, Y. Zhang, T.N. Kim, G.L. Chen, Mater. Lett. **62**, 2673 (2008)
[48] J.M. Zhu, J.L. Meng, J.L. Liang, Rare Met **35**, 385 (2016)
[49] Y.J. Zhou, Y. Zhang, F.J. Wang, Y.L. Wang, G.L. Chen, J. Alloy. Compd. **466**, 201 (2008)
[50] A. Munitz, M.J. Kaufman, M. Nahmany, N. Derimow, R. Abbaschian, Metall. Mater. Trans. A **714**, 146 (2018)

[51] S. Liu, M.C. Gao, P.K. Liaw, Y. Zhang, J. Alloy Compd. **619**, 610 (2015)
[52] S.Q. Xia, M.C. Gao, Y. Zhang, Mater. Chem. Phys. **210**, 213 (2018)
[53] D. Li, Y. Zhang, Intermetallics **70**, 24 (2016)
[54] D. Li, M.C. Gao, J.A. Hawk, Y. Zhang, J. Alloy. Compd. **778**, 23 (2019)